Available online at www.sciencedirect.com
ScienceDirect
Biosensors and Bioelectronics 22 (2007) 1723–1732
BIOSENSORS & BIOELECTRONICS
www.elsevier.com/locate/bios

Self-assembled monolayers of polythiophene conductive polymers improve biocompatibility and electrical impedance of neural electrodes

Alik S. Widge [a,*], Malika Jeffries-El [d], Xinyan Cui [c], Carl F. Lagenaur [b], Yoky Matsuoka [a]

[a] *The Robotics Institute, Smith Hall, Carnegie Mellon University, 5000 Forbes Avenue, Pittsburgh, PA 15217, USA*
[b] *Department of Neurobiology, University of Pittsburgh, Pittsburgh, PA, USA*
[c] *Department of Bioengineering, University of Pittsburgh, Pittsburgh, PA, USA*
[d] *Department of Chemistry, Iowa State University, Ames, IA, USA*

Received 24 March 2006; received in revised form 21 July 2006; accepted 8 August 2006
Available online 2 October 2006

Abstract

There is continued interest in the development of conductive polymer coatings to improve the electrical properties and biocompatibility of electrodes for neural prostheses. We present here a new type of coating, based on mixed self-assembled monolayers (SAMs) of thiolated poly(alkylthiophene)s and functionalized alkanethiols. When assembled as a SAM on electrodes designed for *in vitro* electrophysiology, these polymers are able to significantly lower electrode impedance at 1 kHz. The same mixed formulation is able to promote the outgrowth of neurites from primary mouse cortical neurons when the alkanethiol component is functionalized with a neural cell adhesion molecule (NCAM) binding antibody. Atomic force microscopy of the SAMs shows that they exert their effect through the well-known mechanism of increasing electrode surface area. These new covalently bound films have the potential to be more robust and are more controllable in their composition than existing electrodeposited conductive polymer coatings.
Published by Elsevier B.V.

Keywords: Biocompatibility; Conducting polymer; Neural interface; Neural prosthesis; Self-assembled monolayer

1. Introduction

The prospect of healing damaged nervous systems with implanted electronic devices (commonly referred to as "neural prostheses") continues to stimulate vigorous research activity and has begun to demonstrate some clinical efficacy (Schwartz, 2004; Rutten, 2002; Patterson et al., 2004; Kennedy et al., 2004; Dhillon and Horch, 2005). Although current clinical applications remain limited to control of cursor movement, new end-effector prostheses are being developed to be controlled by neural data (Vande Weghe et al., 2004; Afshar and Matsuoka, 2004; Matsuoka et al., 2006). These devices will require continuous input of high-resolution electrode data. However, even the most advanced electrode systems continue to show a degradation of the interface over time, with individual electrode sites slowly becoming unable to record (Vetter et al., 2004; Carmena et al., 2003; Branner et al., 2004; Rousche and Normann, 1998; Schwartz, 2004). Histological studies suggest that this loss is due to localized chronic inflammation, triggered at least in part by probe micromotion, and have hypothesized that inflammation could be reduced by modifying probe surfaces with biomolecules and decreasing the mechanical mismatch between neural tissue and implant materials (Polikov et al., 2005; Biran et al., 2005; Spataro et al., 2005; Shain et al., 2003). Finite element models of the neural tissue/electrode interface provide support for this hypothesis (Lee et al., 2005; Subbaroyan et al., 2005).

Many methods are known to coat electrode surfaces with soft layers of biomolecules, including hydrogels, layer-by-layer assembly, and multi-layer coupling schemes (Williams et al., 2005; Nyberg et al., 2002; He and Bellamkonda, 2005; Webb et al., 2001; Fernandes et al., 2004). However, such coatings increase the separation between the electrode and the target neuron, and may also increase the electrode impedance; both effects could decrease neural signal strength and ultimately worsen *in vivo* performance. One particularly attractive option is coating electrodes with mixed films of biomolecules and conductive polymers. Such films not only improve electrode biocompati-

* Corresponding author. Tel.: +1 412 268 1858.
E-mail address: alik@cs.cmu.edu (A.S. Widge).

0956-5663/$ – see front matter. Published by Elsevier B.V.
doi:10.1016/j.bios.2006.08.011

bility, but have also been shown to lower electrode impedance, sometimes up to two orders of magnitude (Stauffer and Cui, 2006; Kim et al., 2004; Cui et al., 2001a,b, 2003; Xiao et al., 2004; Cui and Martin, 2003a; Blau et al., 2002). All known conductive polymer coatings for neural probes are created by electrochemical co-deposition of the polymer and a biocompatible anion at individual electrode sites. This process allows tailoring of the film properties at each electrode. However, electrodeposition processes do not permit precise control of either the relative proportion of polymer and biomolecule within the film or the spatial arrangement of these components at the micrometer or nanometer scales. Moreover, because the films are only coupled to the electrode by electrostatic forces, delamination may occur, either due to mechanical forces or to slow attack of the polymer/metal interface by the surrounding electrolyte (Cui and Martin, 2003b). It would therefore be desirable to have a conductive polymer technology that is more tightly bound to the electrode and that allows more control of film composition.

Self-assembled monolayers (SAMs) of organic molecules are an alternative to electrodeposition that may resolve these difficulties. SAMs, which are covalently bound to their substrates, may be formed on most common electrode materials (Bain et al., 1989; Geissler et al., 2004; Li et al., 2003; Harrison et al., 2001; Zhang and Srinivasan, 2004; Veiseh et al., 2004; Shriver-Lake et al., 1997; Lu et al., 2000; Massia et al., 2004). Well-packed SAMs can generally be formed through overnight incubation of the substrate in a dilute organic solution of the assembling molecule. Once formed, SAMs present surface groups that can then be used for covalent coupling of biomolecules (Patel et al., 1997; Su and Li, 2004; Veiseh et al., 2004; Shriver-Lake et al., 1997; Lu et al., 2000; Zhang et al., 2005; Jung et al., 2001; Houseman et al., 2003). SAMs are relatively robust under biological conditions, and their binding to the substrate can often be refreshed electrochemically (Yang et al., 1996, 1997, 2004; Flynn et al., 2003; Sharma et al., 2004; Schneider and Buttry, 1993).

Our proposed technology is based on SAMs containing conductive polymers from the poly(alkylthiophene) family. These polymers have previously been demonstrated to have high conductivity, largely due to the availability of synthesis chemistries that ensure regioregular head-to-tail coupling and high overlap of orbitals along the polymer backbone (McCullough and Ewbank, 1998; McCullough, 1998). Recent work has also demonstrated that they can be customized with a wide variety of functional end-groups, including those that allow self-assembly on metals (Jeffries-El et al., 2004, 2005). By self-assembling these polymers on a metal surface, we hypothesize that we can increase the effective electrode surface area, thus lowering the electrical impedance.

In this paper, we describe our initial characterization of polythiophene SAMs as coatings for neural electrodes and demonstrate that the technology can be competitive with existing coatings. We explore the SAMs' nanoscale topology, biocompatibility with neurons, and ability to modify the properties of *in vitro* neural electrodes. We conclude with proposed physical mechanisms and explanations for the observed effects, and discuss future steps that must be taken to further develop this technology and demonstrate its usefulness.

2. Methods and materials

Characterization of these films proceeded in three stages. First, the ability of polythiophenes to form SAMs was verified by atomic force microscopy (AFM). Second, SAMs functionalized with neural adhesion molecules were cultured with primary mouse neurons to demonstrate biocompatibility. Finally, electrical impedance was measured for SAMs with and without coupled adhesion molecules to show that these coatings are able to improve electrode characteristics. All SAMs were formed using the well-known chemistry of thiol groups binding to clean gold surfaces. For a schematic of the process from SAM formation through cell culture, see Fig. 1.

2.1. Atomically flat gold substrates for atomic force microscopy

Atomically flat Au(1 1 1) surfaces were prepared through a template-stripping procedure adapted from Wagner et al. (1995). Briefly, freshly cleaved ruby mica sheets were heated to 465 °C under vacuum on the stage of a Denton Systems thermal evaporator. 1300 Å of gold (99.99% purity, Kurt J.

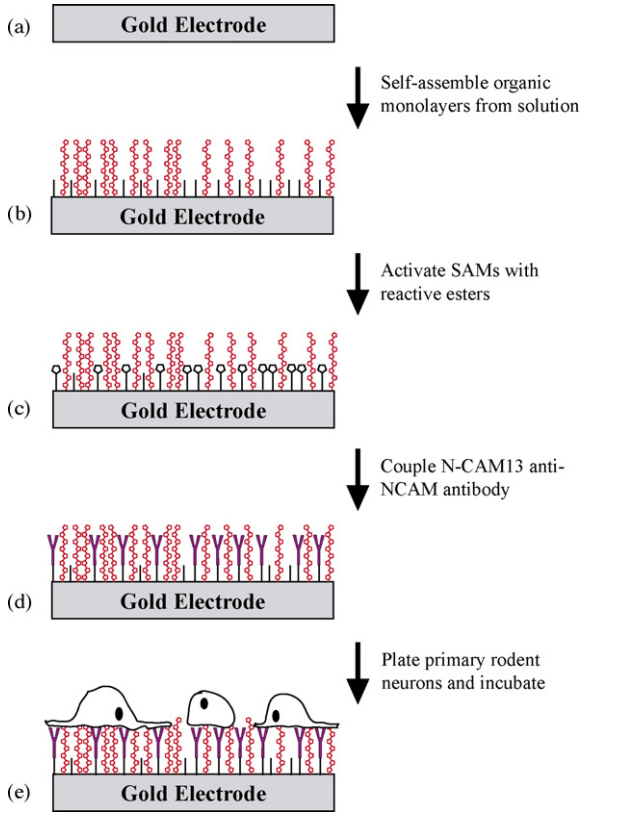

Fig. 1. Assembly schematic for SAM-based neuron/electrode interface. (a and b) Formation of mixed EHPT/MHA SAM by incubation in organic thiol solution; (c) formation of reactive NHS esters on MHA carboxyl groups; (d) capture of adhesion-promoting biomolecules (N-CAM13 anti-NCAM) by NHS ester reaction with free amino groups; (e) quenching of unreacted esters and plating of primary neurons that bind to the coupled adhesion molecules.

Lesker Corporation) were deposited by evaporation from a tungsten boat at a rate of 1 Å/s for the first 200 Å and 3 Å/s thereafter. The deposited gold was further annealed overnight before cooling and removal from the chamber. The mica sheet was then cut into approximately 1 cm squares which were glued to glass coverslips using a solvent-resistant photocurable epoxy (SU-8 2007, Microchem). Cured glass/epoxy/gold/mica "sandwiches" were stored until immediately before use, at which time the mica was delaminated from the gold by gentle mechanical pressure. This produced a clean, flat, crystalline gold surface for SAM formation and visualization.

2.2. Gold-coated coverslips for cell culture

8 mm glass coverslips were cleaned by serial washing in 8N HNO_3, glass-distilled water, acetone (stored over molecular sieves), and absolute ethanol. Dry slips were mounted with polyimide tape onto silicon carrier wafers (Silicon Quest) and placed into the vacuum chamber of the same evaporator used for template-stripped gold deposition. 30 Å of chromium were deposited as an adhesion layer (Cr-coated tungsten rods, Kurt J. Lesker Corporation) followed by 100 Å of gold, without breaking vacuum between films. Both films were deposited at a rate of 2.5 Å/s. These film parameters produce a translucent film that allows monitoring of cultured cells by inverted phase contrast microscopy. Immediately before use, coated coverslips were cleaned by 5 min of oxygen plasma treatment.

2.3. Formation of self-assembled monolayers on gold surfaces

Self-assembled monolayers were formed on gold from solutions containing mixtures of 16-mercaptohexadecanoic acid (MHA, Sigma, received as 90% and recrystallized from HPLC-grade chloroform) and end-thiolated poly(3-(2-ethylhexyl)thiophene) (EHPT, MW approximately 3000 g/mol, synthesized following the method of Jeffries-El et al., 2004). All solutions were prepared in HPLC-grade toluene. Solutions for single-component SAMs were 3 mg/ml of either component (approximately 1 mM in EHPT and 10.4 mM in MHA). Solutions for mixed SAMs contained multiples of these base concentrations; for instance, the 1:2 EHPT:MHA SAM solution was prepared from 3 mg of EHPT and 6 mg of MHA per ml of toluene. The molecular proportions in the final SAM were expected to be different from those in solution. Higher molecular weight compounds chemisorb faster from mixed solutions, leading us to expect enrichment of EHPT over its solution fraction (Choo et al., 2003; Harrison et al., 2001).

Solutions were prepared in glass scintillation vials that were cleaned with a "base piranha" solution (one part 30% hydrogen peroxide, one part ammonium hydroxide, five parts distilled water, heated to 80 °C) to remove all traces of organics, then rinsed thoroughly with distilled water and dried overnight in a 120 °C oven. Gold samples, prepared and cleaned as above, were immersed in SAM-forming solutions for at least 36 h and protected from light during SAM formation.

After SAM formation, substrates were rinsed thoroughly in toluene and chloroform to remove unbound material. They were then soaked for at least 30 min in fresh toluene to further loosen excess molecules, rinsed again in toluene and absolute ethanol, then blown dry with prepurified nitrogen.

2.4. Protein coupling into self-assembled monolayers

Before cell culture, SAMs on gold-coated coverslips were functionalized with protein to allow neuronal adhesion and neurite extension. Following a protocol adapted from Patel et al. (1997) and Su and Li (2004), the COOH terminal groups of MHA were activated to highly reactive NHS esters, which then captured primary amine groups on protein. Briefly, coverslips were immersed for 1 h in an absolute ethanol solution of 45 mM *N*-hydroxysuccinimide (NHS, Sigma) and 68 mM *N*-(3-dimethylaminopropyl)-*N*′-ethylcarbodiimide hydrochloride (EDAC, Sigma). They were then rinsed twice in ethanol, allowed to dry in a sterile polystyrene dish, and spotted with 30 μl each of 100 μg/ml antibody against the neural cell adhesion molecule NCAM (antibody N-CAM13, produced in-house from hybridomas, available from BD PharMingen). N-CAM13 was diluted in phosphate-buffered saline (PBS), pH 7.3, dialyzed against PBS to remove any residual primary amines, and sterilized by filtration through an 0.22 μm syringe filter. Protein coupling was allowed to proceed for 2 h at room temperature in a parafilm-sealed dish, followed by removal of unbound protein by flooding the dish twice with sterile PBS under vigorous agitation. Unreacted NHS esters were quenched by further incubation for at least 30 min in PBS. SAMs of pure EHPT were subjected to this same protocol before culture; while this is not expected to lead to protein coupling, nonspecific adsorption is likely.

Essentially the same protocol was used to protein-functionalize MHA-containing SAMs on template-stripped Au(1 1 1) surfaces. However, the coupled protein was not N-CAM13, but a 100 μg/ml solution of FITC-conjugated goat anti-mouse IgG (Sigma).

2.5. Atomic force microscopy (AFM)

SAMs on template-stripped gold were imaged in tapping mode using a Digital Instruments MultiMode AFM with NanoScope IIIa controller. All scans were performed in a dry nitrogen atmosphere using cantilevers with a nominal force constant of 42 N/m. Driving voltage and deflection setpoints were adjusted to apply the minimum force possible to the sample without causing the AFM control loop to lose surface contact.

2.6. Primary neuron cell culture on SAMs

Biocompatibility of the protein-functionalized EHPT/MHA SAMs was assessed by culture of primary mouse cortical neurons. Timed-pregnant female Swiss Webster mice at 18 days gestation (Charles River Laboratories) were euthanized by CO_2 inhalation and cervical dislocation, followed by harvesting of embryos by Caesarian section and dissociation

of cortical neurons according to the protocol of Schnitzer and Schachner (1981). Cortices were stored for up to 2 days at 4 °C in Hibernate-E medium (BrainBits LLC) supplemented with B-27 and 0.5 mM Glutamax (both from Invitrogen); this medium has previously been demonstrated to permit storage of cortical tissue for up to 1 week without loss of neuronal viability (Brewer and Price, 1996). Dissociation was then performed immediately before plating cells onto SAM-coated substrates.

Cells were counted in a hemocytometer under phase contrast and diluted to a plating concentration of 0.5×10^6 phase-bright cells per ml in Neurobasal medium (Invitrogen) with B-27 and 0.5 mM Glutamax. Coverslips were transferred to a 24-well culture plate, and 0.5 μl of the dilute neuron suspension was plated on each coverslip, corresponding to a density of roughly 250 cells/mm^2. One hour after plating, each well was filled with approximately 0.5 ml of Neurobasal with B-27 and Glutamax. Cultures were maintained at 37 °C in 5% CO_2, and 50% of the medium was replaced after 3 days. All animal protocols were reviewed and approved by the Institutional Animal Care and Usage Committees of both Carnegie Mellon University and the University of Pittsburgh.

2.7. Immunostaining and cell counting

At 3 and 7 days *in vitro* (DIV), coverslips were fixed and stained to assess neurite outgrowth. Cells were fixed for 10 min in 4% paraformaldehyde (Sigma), then immunolabeled for 1 h with a primary rat antibody against the mouse M6 neuronal antigen. Nonspecific binding was blocked by prior incubation with 10% bovine serum and 1% bovine serum albumin in Tris-buffered saline. Following removal of the primary antibody by washing in PBS, stained cells were incubated with a Cy3-labeled goat anti-rat secondary antibody for 1 h.

Neurons were photographed at 400× magnification, with confirmation of neuronal identify by M6 fluorescent staining. Thirty fields were measured for each condition at each time-point, with the fields being drawn from at least three coverslips. Neurite length was measured from captured fluorescence images using the program IPLab (version 3.9.4 r2 for Macintosh), calibrated using an image of a micrometer captured with the same optics. The longest process completely captured within each field was considered to be the primary neurite, and its length was measured from the end of the hillock to the most distal extent of the growth cone. In the event that a single neuron could not be captured within a single image, it was still considered as one field.

Statistical analyses were performed in Microsoft Excel. Overall statistical significance of the results at 3 and 7 DIV was assessed with a one-factor ANOVA; individual groups were then compared by the Neuman–Keuls procedure. Growth within a condition between 3 and 7 DIV was tested with a two-tailed Student's *t*-test for unequal sample variances; no significance level correction was employed, since this set of tests was pre-planned. Our initial hypothesis was that the mixed SAMs tested should show performance somewhere in between that of pure EHPT or MHA SAMs, and that individual conditions should differ from themselves between 3 and 7 DIV.

2.8. Electrical impedance spectroscopy

Impedance measurements were carried out using EcoMEA 60-electrode arrays from MultiChannel Systems. Arrays were cleaned for 5 min under oxygen plasma before being mounted on the stage of the thermal evaporator. The entire array was masked with aluminum foil, except for a central square containing the electrodes. Each array was then coated with 30 Å Cr and 100 Å Au using the same deposition parameters as for gold-coated coverslips. As noted by Nam et al. (2004), this technique coats each electrode and the surrounding area with high-purity gold without shorting electrodes to each other. After gold coating, a glass ring provided by MultiChannel Systems was sealed onto each array using Epo-Tek 353ND epoxy and cured for at least 2 h at 90 °C, thus creating a well for liquid containment. Immediately before use for SAM formation, all arrays were further cleaned by a second 5 min of oxygen plasma treatment. SAMs were formed on MEAs by filling the central well with approximately 1.5 ml of one of the solutions described above. The filled MEA was then incubated for at least 36 h in a sealed jar alongside a vial of toluene that maintained atmospheric saturation and prevented solution evaporation.

After SAM formation, the MEA well was vigorously rinsed at least five times each with toluene and chloroform to remove all unbound material, followed by at least 30 min further incubation with fresh toluene. MEAs were allowed to dry for at least 12 h to minimize solvent trapping in the monolayer. For preparation of protein-coupled SAMs, the well was filled with an NHS/EDAC solution (prepared as above) for 1 h. The solution was drained, the well rinsed thoroughly with absolute ethanol, and a 100 μg/ml solution of FITC-conjugated goat anti-mouse IgG (Sigma) in PBS was spotted onto the gold-coated area. Protein coupling was allowed to proceed for at least 1 h before extensive rinsing of the well with glass-distilled water.

Electrical impedance spectroscopy (EIS) was performed in PBS (pH 7.0) using a Gamry Instruments FAS2/Femtostat potentiostat controlled by the Gamry Framework software. MEAs were mounted using a custom connector that allowed selection of any of the 60 electrodes. A three-electrode cell was used, with an individual MEA electrode as the working electrode, a large-diameter platinum wire as the counter electrode, and a saturated calomel electrode as the reference. Impedance was measured with a 10 mV RMS amplitude sinusoid at a DC bias of 0 V versus the reference electrode, taking four measurements per decade from 100,000 to 10 Hz. Before measurement, all MEAs were allowed to equilibrate overnight in PBS to standardize the SAM hydration state and ensure thorough wetting of all electrode wells; the equilibration PBS was replaced with fresh electrolyte immediately before measurement.

3. Results

3.1. Nanoscale topography of polythiophene SAMs

Tapping mode AFM images of pure and mixed SAMs of EHPT and MHA, along with the bare template-stripped gold

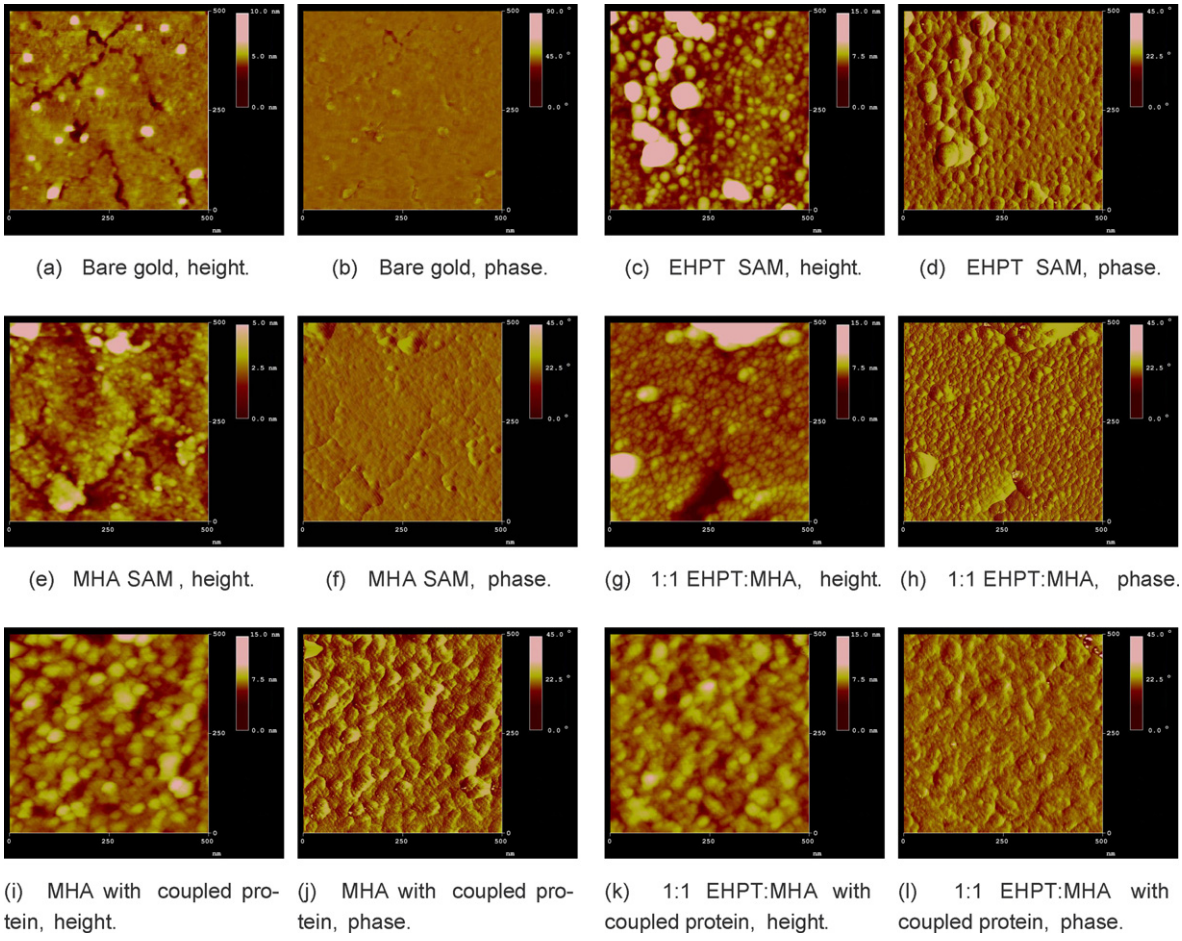

Fig. 2. Atomic force microscopy of pure and mixed EHPT and MHA SAMs on template-stripped Au(1 1 1). All images were acquired in tapping mode with a scan speed of 1 Hz. (a and b) Bare gold. Wide and flat terraces with smaller subgrains are seen; the tall specks are presumed to be dust particles adsorbed to the surface. (c and d) EHPT SAM. The underlying terraces are concealed by this thick, granular film. (e and f) MHA SAM. This tightly packed thin organic monolayer essentially mirrors the underlying terrace structure. (g and h) Mixed 1:1 EHPT:MHA SAM. This strongly resembles an EHPT SAM, with polymer granules seen across the entire surface. Unlike pure EHPT, the underlying gold is not entirely effaced. (i and j) MHA SAM after IgG coupling. Large globular protein molecules (likely including small aggregates) cover the surface. (k and l) Mixed 1:1 EHPT:MHA SAM after protein coupling. The surface now matches the MHA/protein image, showing the same irregularly globular structures.

(TSG) substrate are shown in Fig. 2. As shown in Fig. 2(c) and (d), EHPT SAMs produce a granular surface appearance, with grains roughly 10–20 nm in diameter and with an apparent height of 10–15 nm. The precise height of these grains cannot be determined from these images, as the underlying substrate is effaced. This new roughened surface has an RMS roughness of 1.179 nm (compared to an RMS roughness of 0.481 nm on bare TSG) and a calculated surface area of 260,944 nm^2 in a 500 nm scan square (compared to 253,808 nm^2 for TSG alone).

By contrast, SAMs formed purely from MHA, as shown in Fig. 2(e) and (f), are barely distinguishable from the bare TSG. This is to be expected at the resolution of these scans, since individual MHA molecules are much smaller than our cantilever tip and should form a very tightly packed monolayer that mirrors the underlying topography. MHA's presence is nonetheless verifiable by its ability to participate in protein coupling reactions, the results of which are seen in Fig. 2(i) and (j). After the coupling reaction, the height variation across the surface increases and the underlying gold structure is obscured.

Fig. 2(g) and (h) illustrate the effect of SAM formation from a mixed solution. These images show characteristics of both the MHA and EHPT pure SAMs, but favoring EHPT. The same 10–15 nm tall granules are seen as were found with EHPT, but the fissures between gold terraces are now also visible. Once the protein coupling reaction is performed (Fig. 2(k) and (l)), this surface appears almost identical to a pure MHA SAM with coupled protein.

Although all of the above SAMs were stored in room air (protected from light) for periods of days to months, we did not observe any significant changes over time in the SAM images (data not shown).

3.2. Biocompatibility of SAMs with primary neurons

Fig. 3 displays the biocompatibility of various SAM formulations, as assessed by the willingness of primary neurons to extend neurites on those surfaces. All conditions show continued growth and viability up through 7 DIV, as demonstrated by significant increases in neurite length between these two

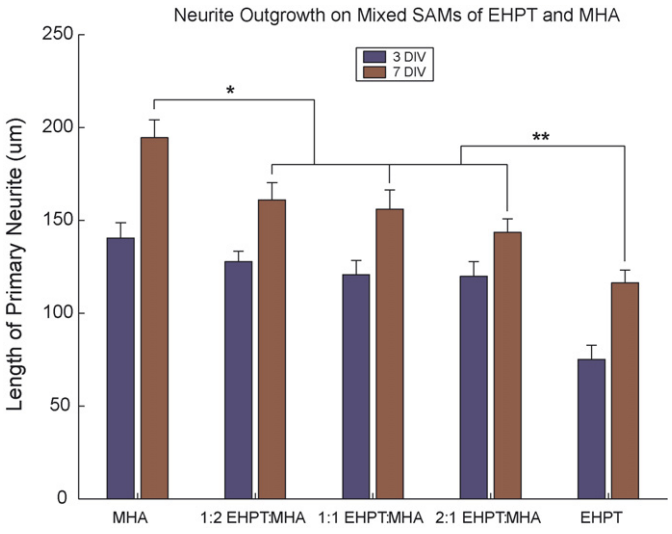

Fig. 3. Outgrowth of neurites on pure and mixed EHPT/MHA SAMs at 3 and 7 DIV. Average length of each cell's primary (longest) neurite is reported. At 3 DIV, only the EHPT group differs significantly from the others ($p < 4.624 \times 10^{-5}$). By 7 DIV, pure MHA shows significantly greater outgrowth than all mixed SAMs ($p < 0.0087$, denoted by *) and pure EHPT (with protein adsorbed) shows significantly less growth ($p < 0.0233$, denoted by **). There is no significant difference at 3 or 7 DIV among the three mixed SAMs tested ($p > 0.3287$).

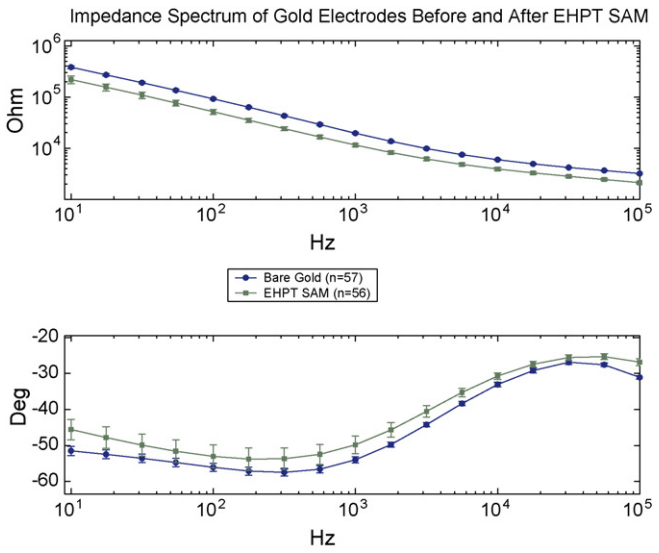

Fig. 5. Impedance of electrodes across an MEA before and after EHPT SAM formation. SAM formation lowers the mean impedance magnitude at 1 kHz by 45% (from 20 to 11 KΩ, $p < 10^{-12}$) and causes a positive phase shift of roughly 4° ($p < 0.0018$).

timepoints ($p < 0.0314$). At 3 DIV, differences between conditions have not fully emerged. The overall ANOVA is significant ($p = 8.213 \times 10^{-8}$), but the only condition that differs from the others in a Neuman–Keuls pairwise analysis is the pure EHPT SAM ($p < 4.624 \times 10^{-5}$). We observed no trend in cell survival on the different SAMs, and there was no significant difference in neuron counts between the EHPT and MHA conditions ($p = 0.7728$ by two-tailed t-test, data not shown). It should be kept in mind that the "pure" EHPT SAM has still been allowed to adsorb N-CAM13. If this adsorption step is eliminated, there is essentially zero survival on that surface.

At 7 DIV, the ANOVA remains significant ($p = 2.155 \times 10^{-7}$), but three levels of outgrowth are now apparent. MHA now shows greater outgrowth compared to any other condition ($p < 0.0087$), and pure EHPT shows significantly less compared to any other ($p < 0.0233$). There is no significant difference between any of the mixed SAM conditions at 3 or 7 DIV ($p > 0.3287$). Although it does appear from Fig. 3 that there is

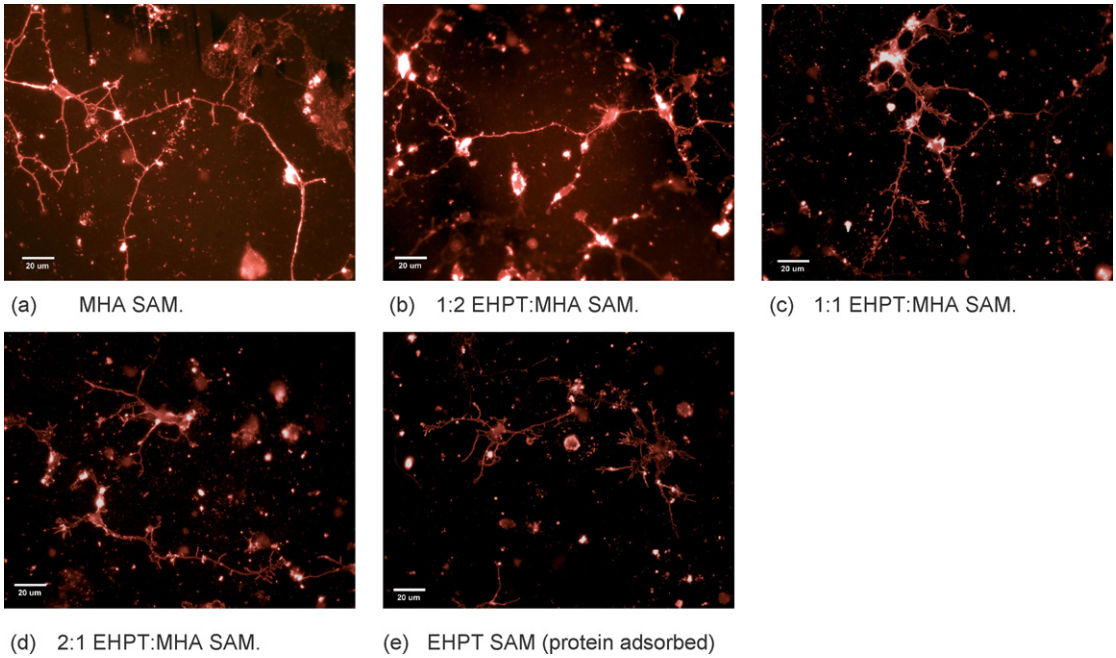

Fig. 4. Fluorescence microscope images of mouse cortical neurons at 3 DIV on the same pure and mixed SAM formulations reported in Fig. 3. All images are 400× magnification with Cy-3 staining against the M6 neural antigen; the scale bar represents 20 μm. As the EHPT:MHA ratio increases, neurite outgrowth decreases. Of particular note is (e), which illustrates the short neurites with broadened growth cones that are common on the pure EHPT SAMs.

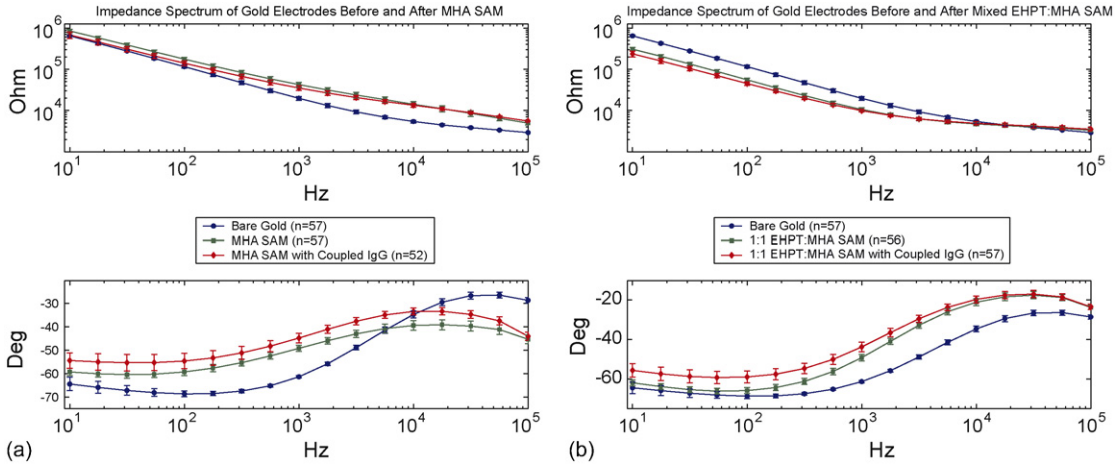

Fig. 6. Impedance spectra of electrodes after coating with a pure MHA SAM (a) or a mixed 1:1 EHPT:MHA SAM (b). The raw MHA SAM more than doubles the impedance magnitude at 1 kHz (from 20 to 42 KΩ, $p < 9.8 \times 10^{-10}$) and causes a significant decrease in electrode capacitance (phase shift from −61° to −49°, $p = 3.5 \times 10^{-9}$). Coupling of protein to this pure MHA SAM causes no significant change in impedance magnitude ($p = 0.0538$) and further shifts the phase (shift of +4°, $p = 0.0005$). The mixed 1:1 SAM lowers impedance approximately 45% (20 KΩ to 11 KΩ, $p < 9.7 \times 10^{-11}$) and shifts the phase positive by 12° (−61° to −49°, $p < 10^{-12}$). Protein coupling to the MHA component of the 1:1 SAM again does not alter the magnitude ($p = 0.3192$), but also further shifts the phase (+5°, $p = 0.0003$).

a trend of increasing outgrowth with increasing MHA content in the mixed SAMs, this is not significant by linear trend analysis ($p > 0.1722$).

The neurite length measurements are reflected in the morphology of cells on the different SAM formulations, as illustrated in Fig. 4. Decreasing MHA (and thus decreasing protein) content can be seen to produce shorter axons and, in the extreme, neurites that are no more than a very broad growth cone.

3.3. Effects of SAM formation on electrode impedance

The impedance spectrum of an EcoMEA before and after pure EHPT SAM formation is shown in Fig. 5. Electrode impedance is significantly lower after coating, by about 40% ($p < 10^{-12}$). A slight phase shift is seen, but the overall shape of the phase curve does not change. To control for mechanisms of impedance change not related to formation of a SAM at the electrode surface, similar MEAs were exposed to pure toluene and to unthiolated EHPT; neither produced any significant change in the impedance spectrum (data not shown).

The pure MHA SAM, as shown in Fig. 6(a), had almost precisely the opposite effect to the pure EHPT SAM. The impedance at the biologically relevant frequency of 1 kHz is now significantly increased by approximately two-fold ($p < 9.8 \times 10^{-10}$). We also see a positive phase shift and flattening of the phase curve, indicating a decrease in electrode capacitance. Addition of coupled protein does not significantly alter the impedance, but does enhance the previously observed phase shift.

EIS of a mixed SAM formed from a 1:1 (w/w) EHPT:MHA mixture in solution is shown in Fig. 6(b). The impedance decrease is almost identical to that caused by pure EHPT, approximately 45% ($p < 9.7 \times 10^{-11}$). The positive phase shift, by contrast, is almost identical to that seen with MHA (+12°, $p < 10^{-12}$), although the curve shape is not visibly altered. Coupling protein to this SAM again does not alter the impedance magnitude, but causes a further positive phase shift just as was seen with MHA.

4. Discussion

4.1. Nanoscale topography of polythiophene SAMs

The AFM results show the expected roughening of the surface by EHPT SAM formation. The observed film morphology is somewhat similar to nonalkylated polythiophene films that have been electrochemically grown from surface-immobilized precursors, although our SAMs are thinner and show a smaller grain size (Kang et al., 2002). Although the images show a grain height of 10–15 nm, this may be an underestimate of the true value, since the force of the cantilever may be perturbing the film even at the low drive voltages used. The grains show a diameter between 10 and 20 nm. Given that the diameter of an EHPT molecule should be on the order of 2 nm, the observed grains are presumed to be aggregates, not single molecules. This is unsurprising, as EHPT is known to form intermolecular aggregates even in dilute solution (Yue et al., 1996).

The mixed 1:1 EHPT:MHA SAM demonstrates the expected effect of EHPT enrichment in the SAM (as compared to its relative concentration in solution). These images do not measure composition, and it is possible that there is substantial MHA present between the EHPT aggregates, but the overall impression from Fig. 2(g) and (h) is of a SAM that is principally EHPT.

4.2. Biocompatibility of SAMs with primary neurons

The results presented in Figs. 3 and 4 demonstrate that mixed SAMs of EHPT and MHA are sufficiently neurocompatible to sustain continued neurite outgrowth up to 7 DIV. As predicted, the quantitative performance of mixed SAMs falls in between that of pure SAMs of either component, and is significantly different from both. While longer-term survival of neurons on

SAMs was not assessed in the present work, our prior experience with primary neuron cultures suggests that a culture lasting until 7 DIV can last indefinitely as long as the medium is regularly changed. The effect of MHA inclusion and NCAM13 coupling is believed to be due to the specific binding of NCAM13 to NCAM on the cultured neurons; our own experience (and that of other groups) is that proteins other than adhesion molecules (e.g., albumin) do not create permissive substrates when coupled.

We were surprised to find no significant difference between any of the mixed SAMs tested. However, this may be explained by the enrichment effect revealed by our AFM investigations. Since EHPT is depositing into the SAM at a faster rate than MHA, the SAMs in the three mixed conditions may be more similar to each other than their forming solutions would suggest.

It should be noted that the NCAM13 coupled to these SAMs is bound in a variety of orientations, and a substantial fraction of the antibodies will not have their active sites available to interact with neurons. This may imply that adequate biocompatibility could be achieved at even higher EHPT:MHA ratios if orientation-specific coupling techniques were used; examples of such techniques are given by Wang et al. (2004) and Hodneland et al. (2002).

4.3. Effects of SAM formation on electrode impedance

The observed 45% impedance decrease after EHPT SAM formation is the trend we would predict, given the increased roughness/surface area seen under AFM. While the AFM data show a surface area change of only 4%, this does not reflect the actual surface area seen by the electrolyte. Mobile ions are able to probe much smaller surface features than are visible to the relatively larger AFM tip, and further study would be necessary to properly correlate AFM measurements with EIS.

The increase in electrode impedance and decrease in effective capacitance after MHA SAM formation is consistent with previous electrochemical studies of alkanethiol SAMs (Mirsky et al., 1997; Yang et al., 1996; Weisshaar et al., 1992; Widrig et al., 1991). The effect can be attributed to a decrease in the double-layer capacitance due to an increased electrode/electrolyte separation, based on the tightly packed and insulating nature of these SAMs. Coupling protein to this SAM produces an impedance decrease that is not significant, but is borderline ($p = 0.0538$). The reason for this decrease is unclear; other authors have attributed it to decreased polarization and diffusion impedances (Darain et al., 2004). It is also possible that the coupled molecules are somehow disrupting the SAM's orderly packing, allowing greater ion permeation through the insulating MHA layer. However, this type of SAM degradation should shift the phase curve back towards the bare-metal baseline, and we observe the opposite.

Based on the EIS results for the two pure SAMs and the prior AFM and cell culture results, one would predict that a 1:1 EHPT:MHA SAM would show characteristics of both components. This is precisely what is observed. We see an impedance decrease that is almost precisely equivalent to that caused by EHPT alone, and a phase shift matching that caused by MHA alone. (The lack of change in the shape of the phase curve shows that performance is not precisely equal to MHA.) Protein coupling behavior also mirrors the MHA SAM.

This result is encouraging, since it implies that we can substantially increase biocompatibility over a pure EHPT SAM without sacrificing the impedance improvement. However, it is also slightly surprising, since one would expect the MHA in the mixed SAM to raise its impedance. We are not currently able to explain this observation. One possibility is that the negative charge of the COOH groups on MHA acts as a dopant for the polythiophene, increasing its conductivity to compensate for the lower amount actually present. Another is that MHA molecules are acting to disrupt the observed EHPT aggregates, which would decrease grain size and increase surface area, again compensating for the lower overall amount of EHPT in the SAM. Equivalent circuit modeling of the pure and mixed SAMs may shed some light on the physical mechanisms underlying the observed spectra. Limited data exist on the equivalent circuits of pure polythiophene or alkanethiol SAMs (Grzeszczuk et al., 1993; Bobacka et al., 1997; Janek et al., 1997). We intend to combine these models and report a more complete analysis of our EHPT-based SAMs in a future paper.

4.4. Conclusions

We have presented results showing that EHPT, when combined with adhesive biomolecules, can form biocompatible SAMs. We have further demonstrated that EHPT-based SAMs can improve the properties of neural stimulating/recording electrodes. Although we have not tested the long-term stability of these SAMs, results from other investigators suggest that the use of further additives and/or a multivalent binding chemistry can produce SAMs that can be stable for months to years (Yang et al., 2004; Letsinger et al., 2000). Thiol-gold bonds are also well known to undergo reductive breaking and oxidative reforming at electrode potentials not far removed from those used in neural stimulation (Yang et al., 1996, 1997; Schneider and Buttry, 1993). This implies that if these SAMs are incorporated into an implanted electrode, it would be possible to "regenerate" the coating in the course of the implant's normal use, further extending the device lifetime.

Moving beyond the homogenous SAMs presented here, a variety of methods are known for producing highly ordered topographies of thiol-based SAMs at extremely fine scales. The well-known technique of microcontact printing has already been used to define protein geometries over microelectrode arrays (Nam et al., 2004; James et al., 2004; Zhang et al., 1999), and this technique is known to also work for printing alkylthiols (Jung et al., 2001; Lahiri et al., 1999) and conductive polymers (Bjornholm et al., 1998; Zhai et al., 2003). Printing has also been demonstrated at the sub-micrometer level, opening the possibility of creating an ordered polymer/biomolecule pattern on the surface of a single microelectrode (Wang et al., 2003). Thiol SAMs are also amenable to other techniques, from photolithography to dip-pen nanowriting, that could also be applied (Ryan et al., 2004; Tarlov et al., 1993; Hacker et al., 2004; Piner et al., 1999). SAM-based patterns can even be combined with topo-

graphic guidance cues to further guide cell behavior (Mrksich et al., 1996).

Although our SAM-based conductive polymer coating produces a smaller impedance decrease than the thicker and rougher electrodeposited films, several mitigating factors make self-assembly a promising coating method for neural prosthetic electrodes. First, these are preliminary results with a polymer that has not been optimized. The side-chain structure could be altered to change the aggregation behavior and/or increase the conductivity. Dopants could also be introduced into the film (possibly coupled to the alkanethiol component) to further improve conductivity. As noted above, one could alter the protein coupling chemistry to be more efficient, thus permitting use of a higher EHPT:MHA ration. The necessary protein content might also be reduced by developing SAMs that present more than one biomolecule, since the presence of multiple neurite growth promoters should cause a synergistic effect (Thelen et al., 2002). Application of such molecular engineering techniques will almost certainly be able to produce SAMs with significantly improved performance.

If a greater surface area is required, other groups have demonstrated electrochemical growth of polythiophenes, including both synthesis from a covalently bound self-assembled initiator and synthesis in a regioregular fashion (Sullivan et al., 2000; Harrison et al., 2001; Kang et al., 2002; Jin et al., 2002). While these techniques are complex due to polythiophene's tendency to overoxidize at potentials very near its synthesis potential, they could be adapted to allow the creation of films that are substantially thicker and rougher while still being chemically bound to the substrate.

Finally, EHPT in particular has unusual solubility properties that were found in previous work to allow it to stably integrate with an artificial lipid bilayer (Widge and Matsuoka, 2004). If this property is also seen with neuronal membranes, EHPT-coated electrodes may be able to sense intracellular voltages without disrupting the membrane, significantly enhancing the capabilities of existing electrode systems.

In summary, these initial results show that polythiophene SAMs are a viable alternative technology for producing conductive polymer coatings on neural electrodes, or for that matter, on any biosensing electrode. We are currently working to characterize the effect of these SAMs on the *in vitro* electrophysiological performance of our coated electrode arrays, and we believe that with further refinement, they will show results that more closely match those of existing technologies.

Acknowledgements

Mr. Widge was funded during the course of this work by a National Defense Science & Engineering Graduate Fellowship and by an individual National Research Service Award fellowship from the National Institute of Neurological Disorders & Stroke. Further support was provided by a seed grant from the American Medical Association Foundation. Ms. Mengyao Zhe of Carnegie Mellon University designed and constructed the custom connector for impedance measurement of multielectrode arrays. Preliminary impedance data were also collected by both Ms. Zhe and Ms. Megan Tzeng, also of Carnegie Mellon. Finally, we thank Dr. James Schneider of the Chemical Engineering Department at Carnegie Mellon for many helpful discussions and the use of multiple pieces of equipment within his laboratory.

References

Afshar, P., Matsuoka, Y., 2004. Proceedings of the 2004 IEEE International Conference on Robotics and Automation, pp. 4633–4638.
Bain, C.D., Troughton, E.B., Tao, Y.-T., Evall, J., Whitesides, G.M., Nuzzo, R.G., 1989. J. Am. Chem. Soc. 111, 321–335.
Biran, R., Martin, D.C., Tresco, P.A., 2005. Exp. Neurol. 195, 115–126.
Bjornholm, T., Greve, D.R., Reitzel, N., et al. 1998., J. Am. Chem. Soc. 120 (30), 7643–7644.
Blau, A., Weinl, C., Mack, J., Kienle, S., Jungc, G., Ziegler, C., 2002. J. Neurosci. Meth. 112 (1), 65–73.
Bobacka, J., Grzeszczuk, M., Ivaska, A., 1997. J. Electroanal. Chem. 427, 63–69.
Branner, A., Stein, R.B., Fernandez, E., Aoyagi, Y., Normann, R.A., 2004. IEEE Trans. Biomed. Eng. 51 (1), 146–157.
Brewer, G., Price, P., 1996. Neuroreport 7 (9), 1509–1512.
Carmena, J.M., Lebedev, M.A., Crist, R.E., O'Doherty, J.E., Santucci, D.M., Dimitrov, D.F., Patil, P.G., Henriquez, C.S., Nicolelis, M.A.L., 2003. PLoS Biol. 1 (2), 193–208.
Choo, H., Cutler, E., Shon, Y.-S., 2003. Langmuir 19 (20), 8555–8559.
Cui, X., Hetke, J.F., Wiler, J.A., Anderson, D.J., Martin, D.C., 2001a. Sens. Actuators A 93, 8–18.
Cui, X., Lee, V.A., Raphael, Y., Wiler, J.A., Hetke, J.F., Anderson, D.J., Martin, D.C., 2001b. J. Biomed. Mater. Res. 56 (2), 261–272.
Cui, X., Martin, D.C., 2003a. Sens. Actuators B 89, 92–102.
Cui, X., Martin, D.C., 2003b. Sens. Actuators A 103, 384–394.
Cui, X., Wiler, J., Dzaman, M., Altschuler, R.A., Martin, D.C., 2003. Biomaterials 24 (5), 777–787.
Darain, F., Park, D.-S., Park, J.-S., Shim, Y.-B., 2004. Biosens. Bioelectron. 19 (10), 1245–1252.
Dhillon, G.S., Horch, K.W., 2005. IEEE Trans. Neural Syst. Rehabilit. Eng. 13 (4), 468–472.
Fernandes, R., Yi, H., Wu, L.-Q., Rubloff, G.W., Ghodssi, R., Bentley, W.E., Payne, G.F., 2004. Langmuir 20 (3), 906–913.
Flynn, N.T., Tran, T.N.T., Cima, M.J., Langer, R., 2003. Langmuir 19 (26), 10909–10915.
Geissler, M., Chem, J., Xia, Y., 2004. Langmuir 20 (17), 6992–6997.
Grzeszczuk, M., Bobacka, J., Ivaska, A., 1993. J. Electroanal. Chem. 362, 287–289.
Hacker, C.A., Batteas, J.D., Garno, J.C., Marquez, M., Richter, C.A., Richter, L.J., van Zee, R.D., Zangmeister, C.D., 2004. Langmuir 20 (15), 6195–6205.
Harrison, K.E., Kang, J.F., Haasch, R.T., Kilbey, S.M. II, 2001. Langmuir 17 (21), 6560–6568.
He, W., Bellamkonda, R.V., 2005. Biomaterials 26, 1990–2983.
Hodneland, C.D., Lee, Y.-S., Min, D.-H., Mrksich, M., 2002. Proc. Natl. Acad. Sci. U.S.A. 99 (9), 5048–5052.
Houseman, B.T., Gawalt, E.S., Mrksich, M., 2003. Langmuir 19 (5), 1522–1531.
James, C.D., Spence, A.J., Dowell-Mesfin, N.M., Hussain, R.J., Smith, K.L., Craighead, H.D., Isaacson, M.S., Shain, W., Turner, J.N., 2004. IEEE Trans. Biomed. Eng. 51 (9), 1640–1648.
Janek, R.P., Fawcett, W.R., Ulman, A., 1997. J. Phys. Chem. B 101 (42), 8550–8558.
Jeffries-El, M., Sauvé, G., McCullough, R.D., 2004. Adv. Mater. 16 (2), 1017–1019.
Jeffries-El, M., Sauvé, G., McCullough, R.D., 2005. Macromolecules 38 (25), 10346–10352.
Jin, S., Cong, S., Xue, G., Xiong, H., Mansdorf, B., Cheng, S.Z., 2002. Adv. Mater. 14 (20), 1492–1496.
Jung, D.R., Kapur, R., Adams, T., Giuliano, K.A., Mrksich, M., Craighead, H.G., Taylor, D.L., 2001. Crit. Rev. Biotechnol. 21 (2), 111–154.
Kang, J.F., Perry, J.D., Tian, P., Kilbey II, S.M., 2002. Langmuir 18 (26), 10196–10201.

Kennedy, P.R., Kirby, M.T., Moore, M.M., King, B., Mallory, A., 2004. IEEE Trans. Neural Syst. Rehabilit. Eng. 12 (3), 339–344.
Kim, D.-H., Abidian, M., Martin, D.C., 2004. J. Biomed. Mater. Res. 71A, 575–585.
Lahiri, J., Ostuni, E., Whitesides, G.M., 1999. Langmuir 15, 2055–2060.
Lee, H., Bellamkonda, R.V., Sun, W., Levenston, M.E., 2005. J. Neural Eng. 2, 81–89.
Letsinger, R.L., Elghanian, R., Mirkin, G.V., Mar, C.A., 2000. Bioconjugate Chem. 11 (2), 289–291.
Li, Z., Chang, S.-C., Williams, R.S., 2003. Langmuir 19 (17), 6744–6749.
Lu, H., Campbell, C., Castner, D., 2000. Langmuir 16 (4), 1711–1718.
Massia, S.P., Holecko, M.M., Ehteshami, G.R., 2004. J. Biomed. Mater. Res. A 68A (1), 177–186.
Matsuoka, Y., Afshar, P., Oh, M., 2006. Neurosurg. Focus 20 (5), E3.
McCullough, R.D., 1998. Adv. Mater. 10 (2), 93–116.
McCullough, R.D., Ewbank, P.C., 1998. In: Skotheim, T.A., Elsenbaumer, R.L., Reynolds, J.R. (Eds.), Handbook of Conducting Polymers. Marcel Dekker, New York, NY, pp. 225–258 (Chapter 9).
Mirsky, V., Riepl, M., Wolfbeis, O., 1997. Biosens. Biolectron. 12 (9–10), 977–989.
Mrksich, M., Chen, C.S., Xia, Y., Dike, L.E., Ingber, D.E., Whitesides, G.M., 1996. Proc. Natl. Acad. Sci. U.S.A. 93, 10775–10778.
Nam, Y., Chang, J.C., Wheeler, B.C., Brewer, G.J., 2004. IEEE Trans. Biomed. Eng. 51 (1), 158–165.
Nyberg, T., Inganäs, O., Jerregard, H., 2002. Biomed. Microdev. 4 (1), 43–52.
Patel, N., Davies, M.C., Hartshorne, M., Heaton, R.J., Roberts, C.J., Tendler, S.J.B., Williams, P.M., 1997. Langmuir 13 (24), 6485–6490.
Patterson, W.R., Song, Y.-K., Bull, C.W., Ozden, I., Deangellis, A.P., Lay, C., McKay, J.L., Nurmikko, A.V., Donoghue, J.D., Connors, B.W., 2004. IEEE Trans. Biomed. Eng. 51 (10), 1845–1853.
Piner, R.D., Zhu, J., Xu, F., Hong, S., Mirkin, C.A., 1999. Science 283 (5402), 661–663.
Polikov, V.S., Tresco, P.A., Reichert, W.M., 2005. J. Neurosci. Meth. 148, 1–18.
Rousche, P.J., Normann, R.A., 1998. J. Neurosci. Meth. 82, 1–15.
Rutten, W.L.C., 2002. Annu. Rev.: Biomed. Eng. 4, 407–452.
Ryan, D., Parviz, B.A., Linder, V., Semetey, V., Sia, S.K., Su, J., Mrksich, M., Whitesides, G.M., 2004. Langmuir 20 (21), 9080–9088.
Schneider, T.W., Buttry, D.A., 1993. J. Am. Chem. Soc. 115 (26), 12391–12397.
Schnitzer, J., Schachner, M., 1981. J. Neuroimmunol. 1, 429–456.
Schwartz, A.B., 2004. Annu. Rev. Neurosci. 27, 487–507.
Shain, W., Spataro, L., Dilgen, J., Haverstick, K., Retterer, S., Isaacson, M., Saltzman, M., Turner, J., 2003. IEEE Trans. Neural Syst. Rehabilit. Eng. 11 (2), 186–188.
Sharma, S., Johnson, R.W., Desai, T.A., 2004. Langmuir 20 (2), 348–356.
Shriver-Lake, L., Donner, B., Edelstein, R., Breslin, K., Bhatia, S., Ligler, F., 1997. Biosens. Biolectron. 12 (11), 1101–1106.
Spataro, L., Dilgen, J., Retterer, S., Spence, A., Isaacson, M., Turner, J., Shain, W., 2005. Exp. Neurol. 194, 289–300.
Stauffer, W.R., Cui, X.T., 2006. Biomaterials 27, 2405–2413.
Su, X.-L., Li, Y., 2004. Biosens. Bioelectron. 19, 563–574.
Subbaroyan, J., Martin, D.C., Kipke, D.R., 2005. J. Neural Eng. 2, 103–113.
Sullivan, J.T., Harrison, K.T., Mizzell, J.P. III, Kilbey, S.M., II 2000. Langmuir 16 (25), 9797–9803.
Tarlov, M.J., Burgess, D.R.F. Jr., Gillen G., 1993. J. Am. Chem. Soc. 115, 5305–5306.
Thelen, K., Kedar, V., Panicker, A.K., Schmid, R.-S., Midkiff, B.R., Maness, P.F., 2002. J. Neurosci. 22 (12), 4918–4931.
Vande Weghe, M., Rogers, M., Weissert, M., Matsuoka, Y., 2004. Proceedings of the 2004 IEEE International Conference on Robotics and Automation, pp. 3375–3379.
Veiseh, M., Wickes, B.T., Castner, D.G., Zhang, M., 2004. Biomaterials 25, 3315–3324.
Vetter, R.J., Williams, J.C., Hetke, J.F., Nunamaker, E.A., Kipke, D.R., 2004. IEEE Trans. Biomed. Eng. 51 (6), 896–904.
Wagner, P., Hegner, M., Güntherodt, H.-J., Semenza, G., 1995. Langmuir 11, 3867–3875.
Wang, H., Castner, D.G., Ratner, B.D., Jiang, S., 2004. Langmuir 20 (5), 1877–1887.
Wang, X., Ryu, K.S., Bullen, D.A., Hua Zhang, J.Z., Mirkin, C.A., Liu, C., 2003. Langmuir 19, 8951–8955.
Webb, K., Caldwell, K., Tresco, P., 2001. J. Biomed. Mater. Res. 54 (4), 509–518.
Weisshaar, D.E., Lamp, B.D., Porter, M.D., 1992. J. Am. Chem. Soc. 114 (14), 5860–5862.
Widge, A., Matsuoka, Y., 2004. Proceedings of the 26th Annual International Conference of the IEEE Engineering in Medicine and Biology Society, pp. 4330–4333.
Widrig, C.A., Chung, C., Porter, M.D., 1991. J. Electroanal. Chem. 310, 335–359.
Williams, J.C., Holecko, M.M. II, Massia, S.P., Rousche P., Kipke, D.R., 2005. J. Neural Eng. 2, L23–L28.
Xiao, Y., Cui, X., Martin, D.C., 2004. J. Electroanal. Chem. 573, 43–48.
Yang, D.-F., Wilde, C., Morin, M., 1996. Langmuir 12 (26), 6570–6577.
Yang, D.-F., Wilde, C.P., Morin, M., 1997. Langmuir 13 (2), 243–249.
Yang, G., Amro, N.A., Starkewolfe, Z.B., Liu, G.-Y., 2004. Langmuir 20 (10), 3995–4003.
Yue, S., Berry, G., McCullough, R., 1996. Macromolecules 29, 933–939.
Zhai, L., Laird, D.W., McCullough, R.D., 2003. Langmuir 19 (16), 6492–6497.
Zhang, F., Srinivasan, M., 2004. Langmuir 20 (6), 2309–2314.
Zhang, S., Yan, L., Altman, M., Lässle, M., Nugent, H., Frankel, F., Lauffenburger, D.A., Whitesides, G.M., Rich, A., 1999. Biomaterials 20, 1213–1220.
Zhang, Z., Yoo, R., Wells, M., Beebe, T.P. Jr., Biran, R., Tresco, P., 2005. Biomaterials 26, 47–61.